Romanian Reports in Physics **71**, 408 (2019)

INTERROGATION METHODS FOR BRAGG FIBER-BASED PLASMONIC SENSORS

V. A. POPESCU

University "Politehnica" of Bucharest, Department of Physics 1,
Splaiul Independentei 313, 060042 Bucharest, Romania
E-mail: *vapopescu@yahoo.com*

Received December 15, 2018

Abstract. The angular and spectral interrogation methods are applied to calculation of the reflectivity, power loss, and spectral and amplitude sensitivities for the *TE*, *TM*, and hybrid modes in a Bragg fiber-based plasmonic sensor with four layers. The results are in agreement with the recent studies of the same structure by using another analytical method, where the electromagnetic field is represented by a Bessel function of the first kind in the core region (SiO_2), a linear combination of Bessel functions of the first and second kinds in the dielectric interior layer (GaP), a linear combination of the Hankel functions in the gold region, and a modified Bessel function of the second kind in the outermost region (H_2O).

Key words: sensors, Bragg fiber, surface plasmon resonance, photonic band gap.

1. INTRODUCTION

During the past few years there was a large interest in studies of plasmonic sensors [1–26] with applications in chemical, biological, and medical sciences. Thus, some plasmonic biosensors [13, 19–20] are applied for detection of human blood groups, and of hemoglobin concentration in human blood and human liver tissues.

The interrogation (angular or spectral) method has been used for the analysis of fiber based plasmonic sensors [22–24] and hollow core Bragg optical fiber [25]. In a recent paper [10] one uses an analytical method, where a linear combination of the Hankel functions H_1 and H_2 represent the field in the gold region of a fiber-based plasmonic sensor. This method was applied for a structure with three, four and five layers [7–9]. When the analyte is the distilled water, the difference between the resonant wavelengths calculated with the finite element method and with the analytical method is very small (0.19 nm for four layers).

In this paper the angular and spectral interrogation methods are applied to a Bragg optical fiber-based plasmonic sensor when the dispersions of SiO_2, GaP, gold and distilled water (H_2O) are considered. The power loss and amplitude sensitivity are increased at optimized thicknesses of the GaP and gold layers for the *TE*, *TM*, and hybrid mode. The results are in agreement with the recent studies of

the same structure by using another analytical method [9] where the field is represented by a Bessel function of the first kind in the core region (SiO_2), a linear combination of Bessel functions of the first and second kinds in the dielectric interior layers (GaP), a linear combination of the Hankel functions in the gold region, and a modified Bessel function of the second kind in the external sensing medium (H_2O).

2. BRAGG FIBER WITH FOUR LAYERS

Figure 1 shows a Bragg fiber with four layers where n_1, n_2, n_3, and n_4 are the refractive indices of the core (SiO_2), GaP, gold, and H_2O, respectively. The thicknesses of the GaP and gold layers are d_2 and d_3, respectively. Figure 2 shows a contour plot of the *z*-component $S_z(x, y)$ of the Poynting vector for the *TE* and *TM* modes at a nonresonant wavelength. The light is incident under the angle α from an air medium in a SiO_2 core of the fiber and the angle inside the fiber is θ. The relation between these angles (Fig. 1) is given by the Snell's law:

$$\frac{\sin\alpha}{\sin(90-\theta)} = \frac{n_1}{n_{air}}, \tag{1}$$

where $n_{air} = 1$ is the refractive index of the air.

The refractive index of the SiO_2 [22], GaP [27], and distilled water [28] materials are calculated through a Sellmeier-type relation. The refractive index of the gold layer is calculated by the Drude model [29] as in references [7–10].

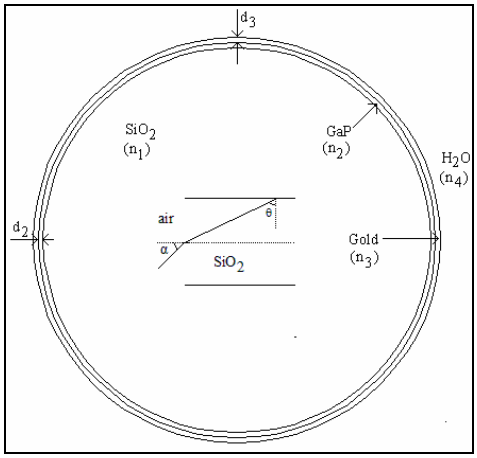

Fig. 1 – Schematic of a Bragg fiber with four layers where n_1, n_2, n_3, and n_4 are the refractive indices of the core (SiO_2), GaP, gold, and H_2O, respectively. The thicknesses of the GaP and gold layers are d_2 and d_3, respectively. The light is incident under the angle α from an air medium in a SiO_2 core of the fiber and the angle inside the fiber is θ.

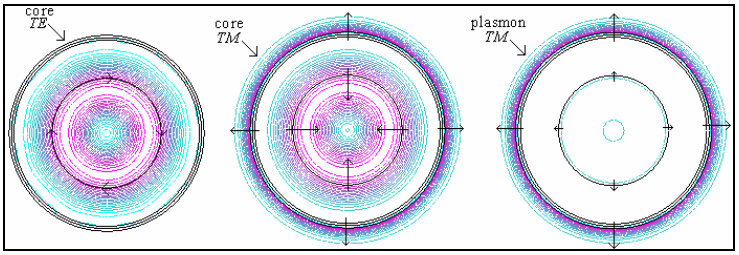

Fig. 2 – Contour plots of the *z*-component $S_z(x, y)$ of the Poynting vector for the *TE* and *TM* modes at a nonresonant wavelength. The arrows indicate the orientation of the electric field for these modes.

3. ADAPTED INTERROGATION METHODS

In the angular interrogation method [24–25], the wavelength is kept constant and the angle of incidence is varied and a sharp dip (maximum of the power loss) appears at a resonance incidence angle θ in the reflectivity. In the spectral interrogation method, the angle of incidence is kept constant and the wavelength is varied. A sharp dip (maximum of the power loss) appears at a wavelength λ in the reflectivity. The resonance incidence angle and the resonance wavelength are dependent on the refractive index of the sensing medium.

The power loss (in dB) for a *TM* mode for a Bragg fiber with $N = 4$ layers is [25–26]:

$$PL(TM) = 10 \log \frac{1}{P(TM)}, \tag{2}$$

and the output power $P(TM)$ is:

$$P(TM) = R(TM)^{\frac{L}{D\tan(\theta)}}, \tag{3}$$

where $R(TM)$ is the corresponding intensity reflection coefficient, L is the sensing length, D is the fiber core diameter, and θ is the angle inside the fiber ($L/D = 25$). Here

$$R(TM) = \left| r(TM) \right|^2, \tag{4}$$

where the amplitude reflection coefficient is:

$$r(TM) = \frac{(M_{11m} + M_{12m} q_{11m}) q_{1m} - (M_{21m} + M_{22m} q_{4m})}{(M_{11m} + M_{12m} q_{11m}) q_{1m} + (M_{21m} + M_{22m} q_{4m})}. \tag{5}$$

In the above relation we have

$$M_m = M_{2m} M_{3m} = \begin{pmatrix} M_{11m} & M_{12m} \\ M_{21m} & M_{22m} \end{pmatrix}, \tag{6}$$

where

$$M_{2m}=\begin{pmatrix}\cos(\beta_2) & -\dfrac{i\sin(\beta_2)}{q_{2m}}\\ -iq_{2m}\sin(\beta_2) & \cos(\beta_2)\end{pmatrix},\ M_{3m}=\begin{pmatrix}\cos(\beta_3) & -\dfrac{i\sin(\beta_3)}{q_{3m}}\\ -iq_{3m}\sin(\beta_3) & \cos(\beta_3)\end{pmatrix}, \tag{7}$$

$$q_{1m}=\frac{\sqrt{n_1^2-n_1^2\sin^2(\theta)}}{n_1^2},\ q_{2m}=\frac{\sqrt{n_2^2-n_1^2\sin^2(\theta)}}{n_2^2}, \tag{8}$$

$$q_{3m}=\frac{\sqrt{n_3^2-n_1^2\sin^2(\theta)}}{n_3^2},\ q_{4m}=\frac{\sqrt{n_4^2-n_1^2\sin^2(\theta)}}{n_4^2}, \tag{9}$$

$$\beta_2=\frac{2\pi d_2}{\lambda}\sqrt{n_2^2-n_1^2\sin^2(\theta)},\ \beta_3=\frac{2\pi d_3}{\lambda}\sqrt{n_3^2-n_1^2\sin^2(\theta)}. \tag{10}$$

4. NUMERICAL RESULTS AND DISCUSSION

Figure 3 shows the contour plot of the *z*-component $S_z(x, y)$ of the Poynting vector at the resonance (λ = 0.6805 μm) between the core-guided *TM* and plasmon *TM* modes for a fiber with four layers made by SiO_2 core (radius r_1 = 1.527 μm) surrounded by a GaP layer (thickness d_2 = 40 nm), a gold layer (thickness d_3 = 40 nm), and by a water layer. Figure 4 shows the reflectivity and power loss *versus* the incident angle α on the core layer (SiO_2) for *TM* mode at λ = 0.62909 μm where *PL* = 127.0848 dB, SNR = 0.21, and FOM = 209.5 RIU^{-1}. The power loss is increased when the reflectivity is decreased.

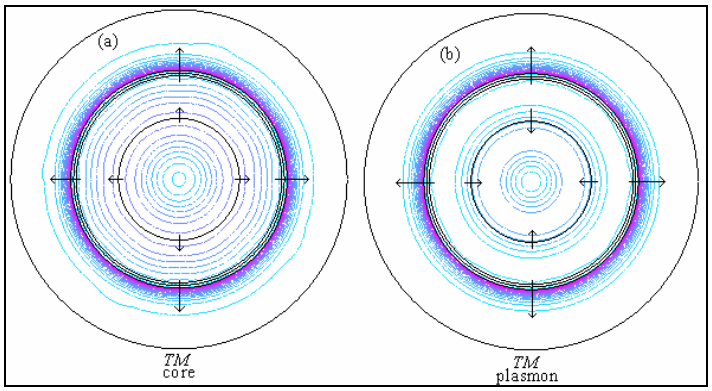

Fig. 3 – Contour plot of the *z*-component $S_z(x, y)$ of the Poynting vector at the resonance (λ = 0.6805 μm) between the core-guided *TM* (a) and plasmon *TM* (b) modes for a fiber with four layers made by SiO_2 core (radius r_1=1.527 μm) surrounded by a GaP layer (thickness d_2 = 40 nm), a gold layer (thickness d_3 = 40 nm), and by a water layer.

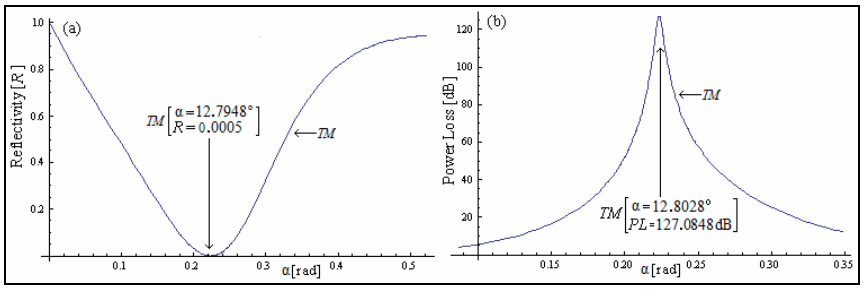

Fig. 4 – Reflectivity (a) and power loss (b) *versus* the angle α for the core modes *TM* of a Bragg fiber ($N = 4$, $d_3 = 40$ nm) at the wavelength $\lambda = 0.62909$ μm.

Figure 5 shows the reflectivity and the corresponding power loss *versus* wavelength for the core modes *TE*, *TM* and *TE* + *TM* for $\alpha = 12.8028^{\circ}$ ($\theta = 81.2526^{\circ}$), near the wavelength $\lambda = 0.62909$ μm. The minimum reflectivity is at the same wavelength as the corresponding maximum power loss for a given mode. For a *TM* mode, the shift towards longer wavelengths of the loss matching point for an increase Δn_a of the analyte refractive index by 0.001 RIU is $\delta\lambda_{res} = 2.89$ nm, the full width at half maximum (*FWHM*) of the loss spectra is $\delta\lambda_{0.5} = 12.5$ nm, the signal-to-noise ratio is *SNR* = 0.23, the figure of merit is *FOM* = 230.7 RIU^{-1}, the maximum of the amplitude sensitivity is $S_A = 413.1$ RIU^{-1}, the maximum value of the power loss is *PL* = 128.2 dB, the angle inside the fiber is $\theta = 81.2526^{\circ}$, the wavelength is $\lambda = 0.629328$ μm and the difference between maximal amplitude sensitivity and resonant wavelengths is $\Delta\lambda_A = 3.5$ nm.

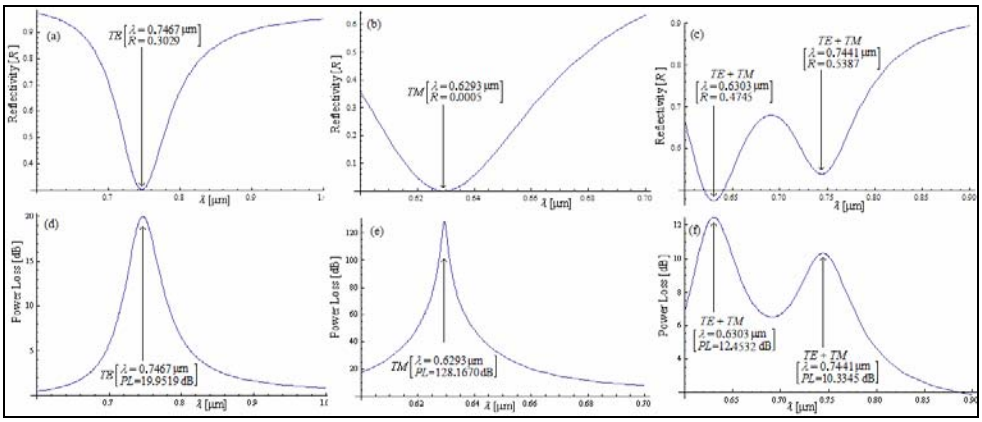

Fig. 5 – Reflectivity (a), (b), (c) and corresponding power loss (d), (e), (f) *versus* wavelength for the core modes *TE*, *TM*, and *TE* + *TM* for $\alpha = 12.8028^{\circ}$ ($\theta = 81.2526^{\circ}$), near the wavelength $\lambda = 0.62909$ μm.

Figure 6 shows the amplitude sensitivity *versus* wavelength for the core modes *TE*, *TM*, and *TE* + *TM* for $\alpha = 12.8028^{\circ}$ ($\theta = 81.2526^{\circ}$) near the wavelength $\lambda = 0.62909$ μm.

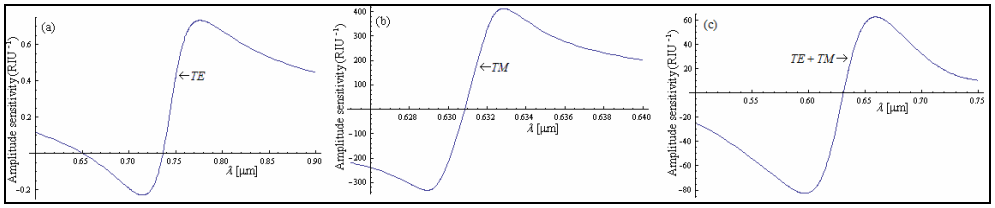

Fig. 6 – Amplitude sensitivity *versus* wavelength for the core modes *TE*, *TM*, and *TE* + *TM* for $\alpha = 12.8028^{\circ}$ ($\theta = 81.2526^{\circ}$) near the wavelength $\lambda = 0.62909$ μm.

Figure 7 shows the reflectivity and power loss *versus* the angle α for the core modes *TM* of a Bragg fiber ($N = 4$, $d_2 = 40$ nm) at the wavelength $\lambda = 0.6805$ μm. It is interesting to note that for the incident angle $\alpha = 18.8565^{\circ}$ on the core layer (SiO_2) and for the corresponding angle $\theta = 77.1725^{\circ}$ inside the fiber at the same wavelength ($\lambda = 0.6805$ μm) one obtains the same values for the power loss ($PL = 116.9938$ dB), signal-to-noise ratio $SNR = 0.11$, and figure of merit $FOM = 112.4$ RIU^{-1}, but different values for the shifts $\Delta\alpha_{res}$ and $\Delta\theta_{res}$ for an increase Δn_a of the analyte refractive index by 0.001 RIU and the full width at half maximum (*FWHM*) of the angular values ($\Delta\alpha_{res} = 0.3311^{\circ}$ and $FWHM = 2.9447^{\circ}$ for α; $\Delta\theta_{res} = 0.2209^{\circ}$ and $FWHM = 1.9630^{\circ}$ for θ).

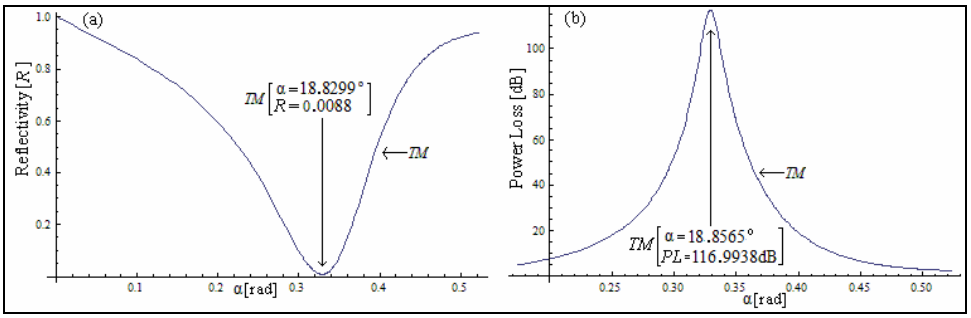

Fig. 7 – Reflectivity (a) and power loss (b) *versus* the angle α for the core modes *TM* of a Bragg fiber ($N = 4$, $d_2 = 40$ nm) at the wavelength $\lambda = 0.6805$ μm.

Figure 8 shows the reflectivity, power loss, and amplitude sensitivity *versus* wavelength for the core modes *TE*, *TM*, and *TE* + *TM* for $\theta = 77.1725^{\circ}$, near the wavelength $\lambda = 0.6805$ μm. For a *TM* mode, the shift towards longer wavelengths of the loss matching point for an increase Δn_a of the analyte refractive index by 0.001 RIU is $\delta\lambda_{res} = 3.94$ nm, the full width at half maximum (FWHM) of the loss spectra is $\delta\lambda_{0.5} = 35.8$ nm, the signal-to-noise ratio is $SNR = 0.11$, the figure of merit is $FOM = 110.1$ RIU^{-1}, the maximum of the amplitude sensitivity is $S_A = 203.1$ RIU^{-1}, the maximum value of the power loss is $PL = 116.99$ dB, the angle inside the fiber is $\theta = 77.1725^{\circ}$, the wavelength is $\lambda = 0.680493$ μm and the difference between maximal amplitude sensitivity and resonant wavelengths is $\Delta\lambda_A = 8.95$ nm. It is important that

real part of the effective index Re (β/*k*) = n_1 sin θ = 1.4557514 sin (77.1725°) = 1.419420 is close to Re (β/*k*) = 1.421346 from the analytical method.

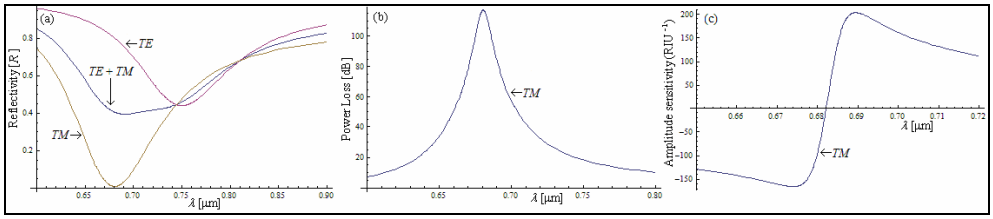

Fig. 8 – Reflectivity (a), power loss (b) and amplitude sensitivity *versus* wavelength for the core modes *TE*, *TM*, and *TE* + *TM* for θ = 77.1725°, near the wavelength λ = 0.6805 μm.

For λ = 0.62909 μm and d_2 = d_3 = 40 nm, r_1 =1.530 μm, the effective index β/*k* of the core and plasmonic mode HE_{11} are 1.446532 + 0.00352789i and 1.4496993 + 0.00356700, respectively. For the same values of λ, d_2, and d_3, but r_1 =1.531μm, the effective index β/*k* of the core and plasmonic mode HE_{11} are 1.446545 + 0.00354053i and 1.4496985 + 0.00355251, respectively. For the same values of λ, d_2, and d_3, but r_1 =1.532 μm, the effective index β/*k* of the core and plasmonic mode HE_{11} are 1.4496979 + 0.00353795i and 1.4465572 + 0.00355323i, respectively. One observe that for r_1 =1.531 μm, there is a loss matching point at λ = 0.62909 μm, where the difference between the imaginary parts of the effective indices of the core and plasmon modes is minimum (0.0000119861).

Figure 9 shows that the real and imaginary parts of the effective index for the core TM_{01} mode are increasing with the radius r_1 of the core layer. Thus for r_1 =1.527 μm, β/*k* = 1.432556 + 0.001523i, and for r_1 =1.800 μm, β/*k* = 1.438243 + 0.002178i when λ = 0.62909 μm and d_2 = d_3 = 40 nm. In the angular interrogation method, the radius of the core layer is absent (but is assumed large) in the calculation of the reflectivity. Thus for λ = 0.62909 μm, r_1 =1.527 μm, r_2 =1.567 μm and r_3 = 1.607 μm, the real part of the effective index is Re (β/ *k*) = $n_1$sinθ = 1.440198, where n_1 = 1.457126 and θ = 81.2264°.

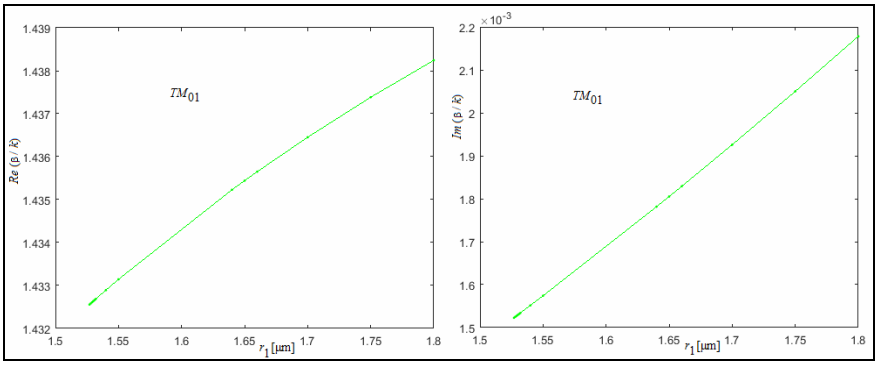

Fig. 9 – The analytical treatment of the real (a) and imaginary (b) parts *versus* the radius of the core layer (r_1) for the core *TM* mode of a Bragg fiber (*N* = 4) at the wavelength λ = 0.62909 μm and d_2 = d_3 = 40 nm.

Figure 10 shows the reflectivity, power loss and amplitude sensitivity *versus* the thickness of the gold layer ($d = d_3$) and of GaP layer ($d = d_2$) for the core *TE*, *TM*, and hybrid *TE* + *TM* modes of a Bragg fiber ($N = 4$) for the angle $\theta = 77.1725^{o}$ at the wavelength $\lambda = 0.6805$ μm. The optimum thicknesses to obtain the minimum reflectivity (the maximum power loss) are: d_2 = 40 nm, d_3 = 42 nm when *PL* =149.4 dB or d_2 = 39 nm, d_3 = 40 nm when *PL* =117.0 dB for the *TM* mode, d_2 = 40 nm, d_3 = 68 nm when *PL* = 6.0 dB or d_2 = 34 nm, d_3 = 40 nm when *PL* =18.9 dB for the *TE* mode and d_2 = 40 nm, d_3 = 42 nm when *PL* = 22.6 dB or d_2 = 34 nm, d_3 = 40 nm when *PL* = 35.0 dB for the hybrid *TE* + *TM* mode. The better values for *PL* are obtained if for fixed values of the thickness d_2, d_3, and θ one evaluates the *PL versus* the wavelength λ. Thus, for a *TM* mode with d_2 = 40 nm, d_3 = 42 nm and $\theta = 77.1725^{o}$, the maximum value of *PL* = 192.6 dB is obtained for $\lambda = 0.678113$ μm, *i.e.* at a shorter wavelength in agreement with the behaviour of HE_{11} mode in the analytical method [9] for an increase of the thickness d_3 of the gold layer.

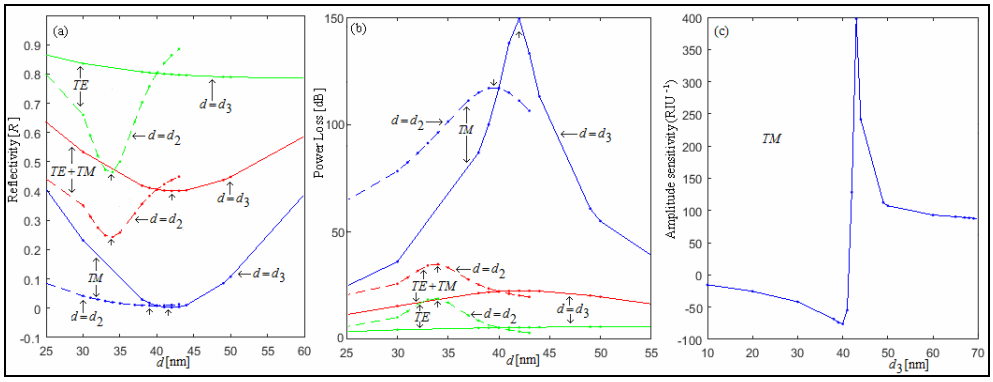

Fig. 10 – Reflectivity (a), power loss (b), and amplitude sensitivity (c) *versus* the thickness of the gold layer ($d = d_3$) and of GaP layer ($d = d_2$) for the core *TE*, *TM*, and hybrid *TE* + *TM* modes of a Bragg fiber ($N = 4$) for the angle $\theta = 77.1725^{o}$ at the wavelength $\lambda = 0.6805$ μm.

In this case the full width at half maximum (*FWHM*) of the loss spectra is $\delta\lambda_{0.5}$ = 15.2 nm, the shift $\delta\lambda_{res}$ = 3.9 nm towards longer wavelengths of the loss matching point for an increase Δn_a of the analyte refractive index by 0.001 RIU, the signal-to-noise ratio *SNR* = 0.26, the figure of merit *FOM* = 258.3 RIU^{-1}, the maximum of the amplitude sensitivity S_A = 617.9 RIU^{-1} and the difference $\Delta\lambda_A$ = 4.2 nm between maximal amplitude sensitivity and resonant wavelengths. For the finite element method [9] we get $\delta\lambda_{res}$ = 3.2 nm, $\delta\lambda_{0.5}$ = 19.4 nm, *SNR* = 0.17, *FOM* = 164.9 RIU^{-1}, and $\Delta\lambda_A$ = 2.1 nm for a HE_{11} mode when r_1 =1.527 μm, r_2 =1.567 μm, r_3 = 1.607 μm ($d_2 = d_3$ = 40 nm) and $\lambda = 0.62909$ μm. The loss matching point ($\lambda = 0.6293$ μm) and the effective index for the core (β/k = 1.449669 + 0.00354217i) and plasmon

(β/k = 1.446438 + 0.00355322i) modes for the mode HE_{11} are calculated by using an analytical method with a step of 0.0001 in the wavelength range. For the same structure [9], the analytical method gives a loss matching point for the core TM_{01} mode at a higher wavelength (λ = 0.6805 μm) and the effective indices for the core and plasmon modes are β/k = 1.421346 + 0.00341024i and β/k = 1.438907 + 0.00341046i, respectively. In this case, $\delta\lambda_{res}$ = 6.0 nm (686.5 nm – 680.5 nm), $\delta\lambda_{0.5}$ = 99.5 nm, *SNR* = 0.06, *FOM* = 60.3 RIU^{-1} and the power loss (2735.0 dB/cm) for the core TM_{01} mode is very large. It is interesting to note that if in the angular method one replace L/D = 25 with L/D = 355, where L is the sensing length and D is the fiber core diameter one obtains a power loss *PL* = 2735.2 dB at the same wavelength (λ = 0.678113 μm) as for L/D = 25, but the maximum of the amplitude sensitivity is unchanged (S_A = 617.9 RIU^{-1} at λ = 0.68234 μm).

Table 1 shows the shift $\delta\lambda_{res}$ towards longer wavelengths of the loss matching point for an increase Δn_a of the analyte refractive index by 0.001 RIU, the full width at half maximum (*FWHM*) of the loss spectra $\delta\lambda_{0.5}$, the signal-to-noise ratio *SNR*, the figure of merit *FOM*, the maximum of the amplitude sensitivity S_A, the maximum value of the power loss *PL*, the angle inside the fiber θ, the wavelength λ, and the difference $\Delta\lambda_A$ between maximal amplitude sensitivity and resonant wavelengths.

Table 1

Values of $\delta\lambda_{res}$ [nm], $\delta\lambda_{0.5}$ [nm], *SNR*, *FOM* [RIU^{-1}], S_A [RIU^{-1}], *PL* [dB], θ [deg], λ [μm], and $\Delta\lambda_A$ [nm] for a *TM* mode of a optical fiber with four layers with the thicknesses d_2 [nm] and d_3 [nm] of the GaP and gold layers, respectively

d_2; d_3	$\delta\lambda_{res}$	$\delta\lambda_{0.5}$	*SNR*	*FOM*	S_A	*PL*	θ	λ	$\Delta\lambda_A$
40; 40	2.9	12.5	0.23	230.7	413.1	128.2	81.2526	0.629328	3.5
40; 40	3.9	35.8	0.11	110.1	203.1	117.0	77.1725	0.680493	9.0
40; 42	3.9	15.2	0.26	258.3	617.9	192.6	77.1725	0.678113	4.2

5. CONCLUSIONS

The results obtained by using the interrogation method are in agreement with the recent studies of the same structure by using another analytical method [7], where the electromagnetic field is based on the Bessel functions. Thus, for a *TM* mode with d_2 = 40 nm, d_3 = 42 nm and θ = 77.1725°, the maximum value of *PL* = 192.6 dB is obtained for λ = 0.678113 μm, *i.e.* at a shorter wavelength in agreement with the behavior of the HE_{11} mode in the analytical method [9] for an increase of the thickness d_3 of the gold layer. Also, the amplitude sensitivity for the core modes near the maximum power loss point for the Bragg fiber with a gold layer is increased for optimized thicknesses of the GaP and gold layers.

REFERENCES

1. V. A. Popescu, N. N. Puscas, and G. Perrone, J. Opt. Soc. Am. B **29**, 3039 (2012).
2. V. A. Popescu, Mod. Phys. Lett. B **26**, 1250207 (2012).
3. V. A. Popescu, Mod. Phys. Lett. B **27**, 1350038 (2013).
4. V. A. Popescu, N. N. Puscas, and G. Perrone, Eur. Phys. J. D **67**, 215 (2013).
5. V. A. Popescu, N. N. Puscas, and G. Perrone, Eur. Phys. J. D **68**, 229 (2014).
6. V. A. Popescu, N. N. Puscas, and G. Perrone, J. Opt. Soc. Am. B **31**, 1062 (2014).
7. V. A. Popescu, N. N. Puscas, and G. Perrone, J. Opt. Soc. Am. B **32**, 473 (2015).
8. V. A. Popescu and N. N. Puscas, Rom. Rep. Phys. **67**, 500 (2015).
9. V. A. Popescu, N. N. Puscas, and G. Perrone, Plasmonics **11**, 1183 (2016).
10. V. A. Popescu, N. N. Puscas, and G. Perrone, Mod. Phys. Lett. B **30**, 1650075 (2016).
11. V. A. Popescu, Rom. J. Phys. **62**, 204 (2017).
12. V. A. Popescu, N. N. Puscas, and G. Perrone, Plasmonics. **12**, 905 (2017).
13. V. A. Popescu, Plasmonics. **12**, 1733 (2017).
14. V. A. Popescu, N. N. Puscas, and G. Perrone, J. Opt. **19**, 075004 (2017).
15. V. A. Popescu, N. N. Puscas, and G. Perrone, Optics **6**, 21 (2017).
16. V. A. Popescu, Rom. Rep. Phys. **70**, 404 (2018).
17. V. A. Popescu, J. Phys. Commun. **2**, 015029 (2018).
18. V. A. Popescu, Proc. Romanian Acad. A **19**, 345 (2018).
19. V. A. Popescu, Plasmonics **13**, 575 (2018).
20. V. A. Popescu, Plasmonics **13**, 1507 (2018).
21. V. A. Popescu and A. K. Sharma, OSA Continuum **1**, 496 (2018).
22. A. K. Sharma, R. Jha, and B. D. Gupta, Opt. Commun. **274**, 320 (2007).
23. A. K. Sharma and G. J. Mohr, New J. Phys. **10**, 023039 (2008).
24. B. D. Gupta and R. K. Verma, J. Sens. **979761**, 1 (2009).
25. V. A. Popescu, Rom. J. Phys. **64**, 202 (2019).
26. A. K. Sharma, A. Dominic, B. Kaur, and V. A. Popescu, submitted to J. Lightwave Technol.
27. F. L. Madarasz, J. O. Dimmock, N. Dietz, and K. L. Bachmann, J. Appl. Phys. **87** 1564 (2000).
28. M. Daimon and A. Masumura, Appl. Opt. **46**, 3811 (2007).
29. M. A. Ordal, L. L. Long, R. J. Bell, S. E. Bell, R. R. Bell, R. W. Alexander Jr., and C. A. Ward, Appl. Opt. **22**, 1099 (1983).